

## Experimental testing of a self-centring concentrically braced steel frame

Gerard J. O'Reilly <sup>a,\*</sup>, Jamie Goggins <sup>b</sup>

<sup>a</sup> Centre for Training and Research on Reduction of Seismic Risk (ROSE Centre), Scuola Universitaria Superiore IUSS Pavia, Italy

<sup>b</sup> MaREI Centre, Ryan Institute & School of Engineering, National University of Ireland, Galway, Ireland

### ARTICLE INFO

#### Keywords:

Self-centring

Concentrically braced frame

Seismic design

Post-tensioning

Tubular members

### ABSTRACT

Conventional concentrically braced frames (CBFs) undergo many cycles of inelastic deformation during seismic excitation. This inelastic deformation leads to the possibility that a structure will remain in an out-of-plumb position, even if it has performed as required by current design codes. This paper presents an improved steel braced framing system that eliminates such residual deformations in the structure by using a post-tensioning arrangement to ensure the structure self-centres following an earthquake. This is achieved by combining the bilinear elastic rocking response of a post-tensioned frame with the inelastic behaviour of tubular steel bracing members to give a system that both dissipates hysteretic energy and ensures self-centring behaviour, termed the self-centring concentrically braced frame (SC-CBF). This SC-CBF system distinguishes itself from previous self-centring CBFs by employing post-tensioned rocking beam-column connections as opposed to a globally uplifting frame. The mechanics behind the behaviour of the SC-CBF are first described, followed by a discussion of an experimental test setup to validate the concept under quasi-static cyclic testing. Results from a total of nine tests are presented to demonstrate the self-centring behaviour of the SC-CBF. Comparisons with analytical expressions developed for the system demonstrate the SC-CBF performs as anticipated and presents a novel system for the seismic design of steel structures.

### 1. Introduction

Concentrically braced frames (CBFs) have been a popular system for resisting the lateral forces exerted by major earthquakes on a structure. This is primarily due to the high lateral stiffness offered by a typical CBF, which limits the amount of lateral drift experienced by a structure. Modern seismic design codes, such as Eurocode 8 (EC8) [1], aim to limit this drift under serviceability limit state conditions, while recent research [2,3] has shown the importance of also limiting floor accelerations amongst other parameters. Khatib *et al.* [4] reported that up until the 1970s, the developments in the seismic response of braced frames had progressed slowly, but the expansion of offshore structures in seismic areas had stimulated investigations into the behaviour of these frames. Since then, a vast amount of data has been amassed to discuss the design and performance of steel braced frames [5–11], describe diagonal tubular member behaviour [12,13,22,14–21], gusset plate behaviour [23–31], and also shake table and hybrid testing [32–38].

Following numerous cycles of inelastic deformation, there is a large possibility of residual deformations being present in the structure. This is despite the system having performed exactly as intended, since design

codes typically aim to limit the amount of lateral deformation during an earthquake and capacity to resist collapse without considering the final state of the structure. These residual deformations, or drifts, can be extremely problematic given the difficulties associated with attempting to straighten a structure following a seismic event. McCormick *et al.* [39] reported that the residual drifts present in a 17 storey steel moment frame building after the 1995 Northridge earthquake in the US went unnoticed during the assessment of the building and were only discovered when the elevators failed to operate because of out-of-plumbness during the re-occupancy. In addition to this, McCormick *et al.* [39] reported that at a hearing of 100 residents in Ashiya city in Japan after the 1995 Hyogoken-Nanbu earthquake, residents reported being conscious of inclinations between 0.005 and 0.006 rad, with inclinations of 0.008 rad causing serious consciousness of the inclination along with dizziness and headaches. Moreover, the presence of residual deformations in structures may also contribute the expected monetary losses of a building, as excessive deformations may lead to the buildings being demolished and rebuilt as opposed to repaired or straightened. FEMA P58 [40] uses the maximum residual drift ratio, together with a building repair fragility, to determine if repair is practicable. O'Reilly *et al.* [41]

\* Corresponding author.

E-mail addresses: [gerard.oreilly@iusspavia.it](mailto:gerard.oreilly@iusspavia.it) (G.J. O'Reilly), [jamie.goggins@nuigalway.ie](mailto:jamie.goggins@nuigalway.ie) (J. Goggins).

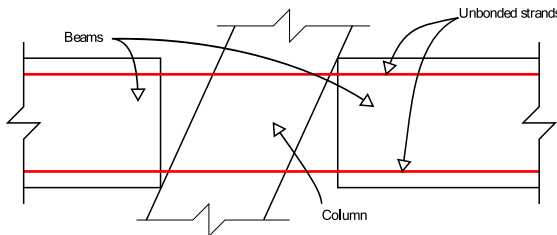


Fig. 1. PRESSS frame rocking system.

illustrated how the contribution to expected loss from demolition due to excessive residual drifts were notable at shaking return periods close to those used in design. Furthermore, Elwood *et al.* [42] noted a disproportionate level of building demolition following the Canterbury earthquakes of 2011 and 2012 in New Zealand, despite rather low damage ratios being reported in many instances. Clearly, residual drifts warrant serious consideration from a post-event occupancy perspective when examining the response of CBFs to seismic loading. However, there is no specific guidance in the European seismic design code, Eurocode 8 [1], on specifications for residual drift limits, although the amount of permanent drift is linked to the state of damage of the structure defined through three limit states in the fundamental performance requirements set out in Section 2 of the code. Nevertheless, a limit of 0.002 rad could be considered for the relative inclination of a column in building after an earthquake. This matches the limits specified in EN 1090-2 [43] for 'as built' imperfection tolerances in design, where compliance guarantees that frame deviations will not cause secondary forces greater than those allowed for in the design. This limit also matches the observations of McCormick *et al.* [39].

During the 1990s, a research programme known as PRESSS (PREcast Seismic Structural Systems) was undertaken in the US and Japan with the goal of developing a low-cost, code-compliant precast concrete building capable of withstanding large lateral displacement with minimum damage [44]. The result was a hybrid system that re-centred itself after seismic loading by means of an internal post-tensioning system. This system is illustrated in Fig. 1, where the beams and columns are

allowed to rock against each other during seismic loading. The unbonded strands remain elastic at all times and, hence, provide an elastic restoring force for the system due to their elongation during gap opening between the beam ends and column face. The energy dissipation comes in the form of specialised elements designated to undergo inelastic behaviour during rocking, which in turn dissipates energy from the system, while the beam and columns remain elastic. The force-deformation behaviour of this system is shown in Fig. 2, where the combination of the two systems working together leads to the so-called 'flag-shaped' behaviour. This self-centring system was initially developed for concrete systems, but has gradually been applied to steel systems such as moment resisting frames [45–47], bracing devices [48] and also steel plate shear walls [49]. More recently, various self-centring steel braced framed systems have been developed, such as a post-tensioned self-centring yielding brace system (PT-SCYBS) [50], self-centring energy dissipation (SCED) brace system [51–56] and a novel self-centring tension-only braces (SC-TOBs) system [57]. This paper develops an alternative novel CBF system into one with the same desirable characteristics as a conventional system but also exhibits a self-centring behaviour. This is described here by first developing the concept in terms of its hysteretic behaviour, followed by a series of quasi-static cyclic experimental tests to validate the concept.

## 2. Behaviour of a self-centring concentrically braced frame (SC-CBF)

### 2.1. SC-CBF arrangement

Numerous different systems for self-centring to achieve the flag-shaped hysteresis loop have been discussed in the literature [45,46,63,47–49,58–62]. These systems comprise two components: a post-tensioning (PT) arrangement, or method of re-centring; and a method of energy dissipation. The former may be achieved by having PT elements running down the length of a building vertically to achieve entire building rocking behaviour, or to place the PT elements along the beams to achieve a rocking connection type behaviour (Fig. 1). For this proposed self-centring concentrically braced frame (SC-CBF), the

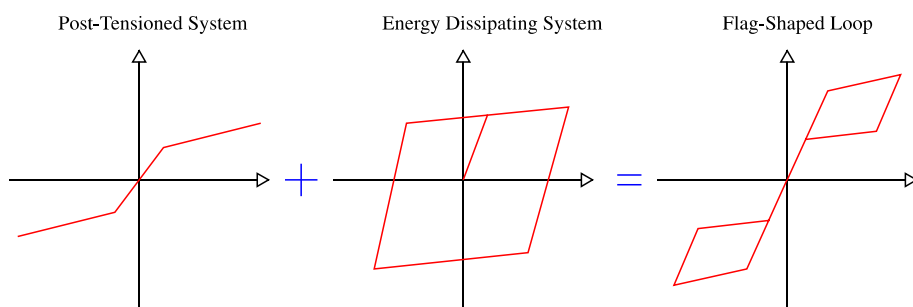


Fig. 2. Composition of a flag-shaped hysteretic loop.

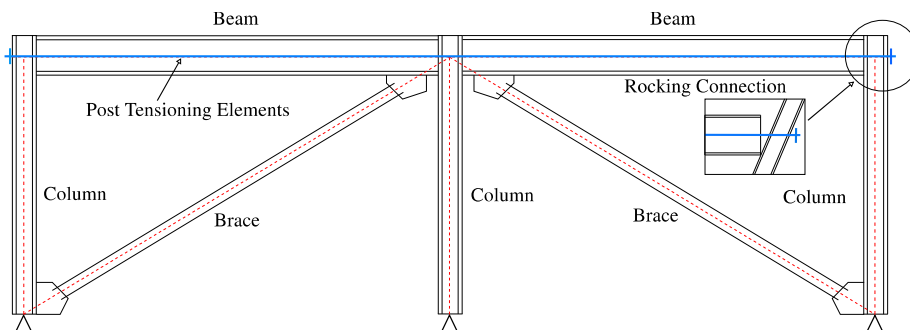
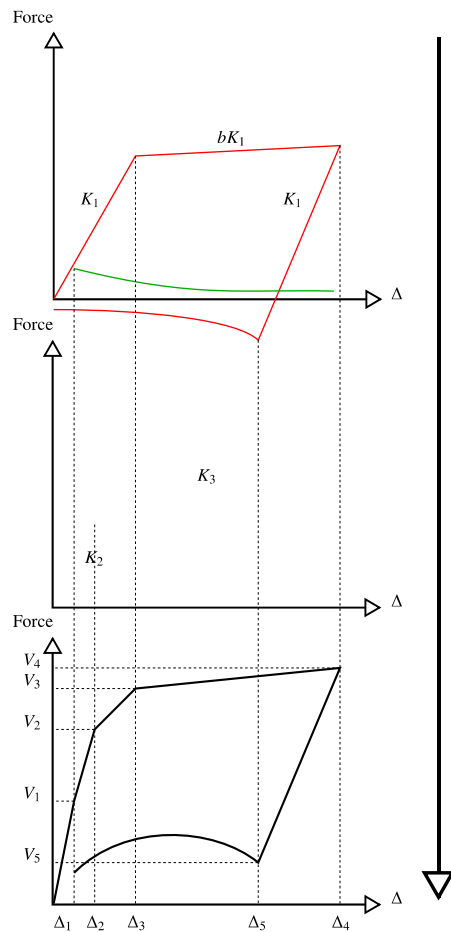


Fig. 3. Schematic of proposed self-centring concentrically braced frame (SC-CBF).



**Fig. 4.** Hysteresis of proposed self-centring concentrically braced frame (SC-CBF) [62].

rocking connection employed by Christopoulos *et al.* [61] is utilised as a self-centring mechanism. The lateral movement of the frame imposes axial deformations on the diagonal bracing members, which results in the tensile yielding and compressive buckling of the braces. The general concept developed in O'Reilly [62] is depicted in Fig. 3 and should not be confused with the self-centring system of the following the same abbreviation previously studied by Roke *et al.* [59,60] which employs a rocking mechanism and energy dissipation at the base of the structure. As shown, the SC-CBF system presented in this paper employs diagonal brace members as its energy dissipating mechanism, which in post-earthquake scenarios would need to be replaced. Aside from typical access obstacles (i.e. non-structural partition elements) encountered during post-earthquake repair of hysteretic dampers, these braces are relatively simple as they are bolted into the frame system and can be easily substituted. This will be seen through the experimental campaign discussed in the following sections, where a series of 8 specimens were tested and replaced with relative ease due to the self-centring nature of the SC-CBF system.

In terms of hysteretic behaviour, the lateral movement of the frame will induce forces in both braces, causing the tension brace to yield and dissipate energy, and the compression member to buckle, dissipating little energy depending on its normalised slenderness,  $\lambda_{zz}$ . The rocking connection behaviour depends on the beam-column connection movement during lateral displacement. Initially, the connection is held closed by the initial axial force in the PT strands and the frame behaves essentially as a moment resisting frame. When the bending moment generated at the connection is larger than this compression moment created by the PT strands, the connection begins to open. This is termed decompression and results in a bilinear elastic hysteretic response. The

hysteretic behaviour of the system is examined and Fig. 4 describes the combined system component response to give the SC-CBF behaviour.

In order to achieve this type of flag-shaped behaviour, a critical assumption is made about the behaviour of the bracing members, which is that the compressive resistance of the brace is relatively small in comparison to its tensile capacity. This has been shown to be the case through shake table testing of CBFs [7,25,26,33]. Elghazouli *et al.* [33] performed numerous shake table tests on braces with a  $\lambda_{zz}$  outside EC8's specified range of 1.3–2.0 for diagonal CBF members, and reported satisfactory behaviour. Goggins *et al.* [64] concluded that despite the lower energy dissipation of the slender braces, they demonstrated a higher fracturing resistance along with other design advantages like the use of tension-only design. Considering these, brace members with a relatively high  $\lambda_{zz}$  can therefore be employed along with a PT arrangement to give the SC-CBF system. Fig. 4 shows the lateral resistance,  $V$ , of the SC-CBF against the roof lateral displacement,  $\Delta$ . The points numbered 1 through 5 denote: 1) compressive brace buckling; 2) PT connection decompression; 3) tensile brace yielding; 4) maximum displacement demand; 5) load cycle reversal and buckling on brace previously in tension.

## 2.2. SC-CBF hysteretic behaviour

Expressions that describe the behaviour shown in Fig. 4 are developed in O'Reilly [62] for the schematic frame shown in Fig. 3 and are described here. The lateral stiffness provided by each of the bracing members in tension can be derived as:

$$K_1 = k_{br} \cos^2 \alpha = \frac{EA_{br}}{L} \left( \frac{B}{L} \right)^2 = \frac{EA_{br} B^2}{L^3} \quad (1)$$

where  $k_{br}$  and  $A_{br}$  are the axial stiffness and cross-sectional area of the bracing member, respectively,  $\alpha$  is brace angle with respect to horizontal,  $E$  is the Young's modulus,  $B$  is the bay width and  $L$  is the brace length. This stiffness represents both the braces loaded in tension and compression, although due to the low buckling resistances of the brace members employed in the SC-CBF, the lateral stiffness of the compression brace may be ignored (i.e. point 1 in Fig. 4 may be omitted) [22,33]. The lateral displacement at which the tensile brace members begin to yield is derived as shown below. For a single frame bay of width  $B$  and height  $H$  with a brace of length  $L$  elongated to a yield strain  $\epsilon_y$  corresponding to a global lateral displacement  $\Delta_3$ , the following expression can be written:

$$(L + \epsilon_y L)^2 = (B + \Delta_3)^2 + H^2 \quad (2)$$

and expanded to:

$$L^2 + 2\epsilon_y L^2 + \underline{\epsilon_y^2 L^2} = B^2 + 2B\Delta_3 + \underline{\Delta_3^2} + H^2 \quad (3)$$

Cancelling the underlined terms, where  $L^2 = B^2 + H^2$  and taking  $\epsilon^2$  and  $\Delta^2$  to be  $\approx 0$ , it can be simplified to the following:

$$\underline{L^2} + 2\underline{\epsilon_y L^2} + \underline{\epsilon_y^2 L^2} = \underline{B^2} + 2\underline{B\Delta_3} + \underline{\Delta_3^2} + \underline{H^2} \quad (4)$$

$$\epsilon_y L^2 = B\Delta_3 \quad (5)$$

$$\Delta_3 = \frac{f_y L^2}{BE} \quad (6)$$

where  $f_y$  is the brace steel yield strength. Assuming a bilinear force-displacement relationship, the post yield stiffness of the brace in tension is given as  $bK_1$ , where  $b$  represents the strain hardening of the brace material.

For the PT frame shown in Fig. 3, the PT connection acts as if it were fully rigid at each connection in the elastic range of loading. It is upon decompression that the frame acts more like a pinned frame, with a rotational stiffness at the gap-opening connections. Up until

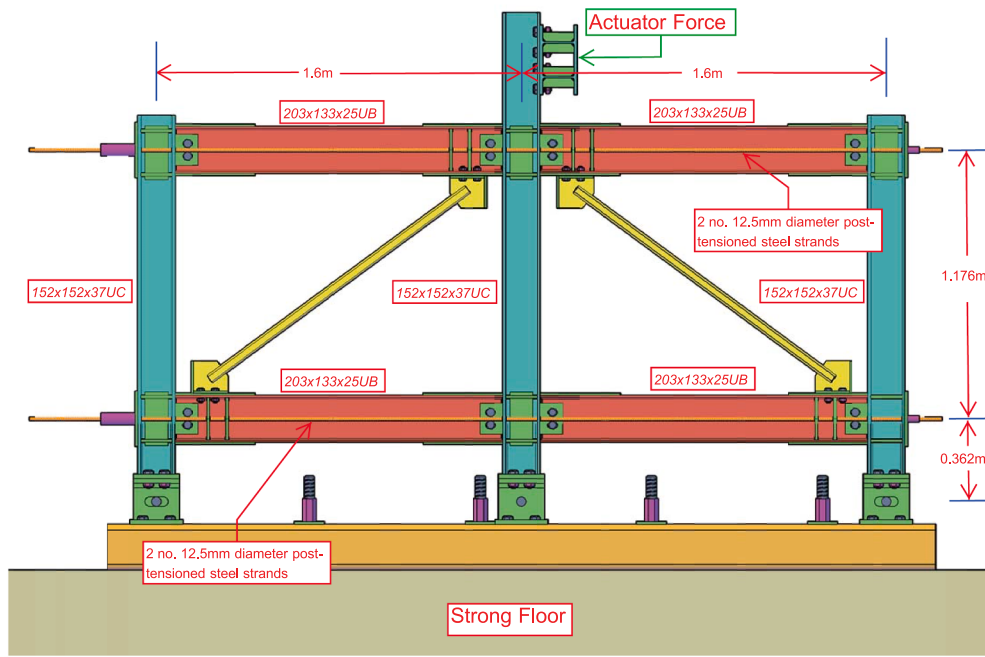


Fig. 5. Front elevation of test frame.

decompression of the connections occurs, the stiffness of the SC-CBF contribution from the frame is effectively the elastic horizontal stiffness of the frame. For a two-bay frame, such as that shown in Fig. 3, the horizontal stiffness can be derived [62] as:

$$K_2 = \left( \frac{H^3}{8EI_c} + \frac{H^2B}{24EI_b} \right)^{-1} \quad (7)$$

where  $H$  is the storey height and  $E$ ,  $I_b$  and  $I_c$  are the Young's modulus, beam and column's second moment of areas, respectively. The decompression bending moment in each connection,  $M_c$ , is given by:

$$M_c = \frac{P_{T0}h_b}{2} \quad (8)$$

where  $P_{T0}$  is the initial post-tensioning applied to the PT elements and  $h_b$  is the beam height. The moment at the four connections in the frame shown in Fig. 3 is then the total overturning moment required to achieve decompression at the rocking connections. Thus, the displacement at decompression can be written:

$$4M_c = K_2\Delta_2H \quad (9)$$

$$\Delta_2 = \frac{2P_{T0}h_b}{K_2H} \quad (10)$$

To determine the post decompression stiffness,  $K_3$ , of the PT frame, the gap opening and subsequent expansion behaviour of the frame need to be considered. During the rocking of the connection, a gap opens up and induces forces in the exterior columns but also in the PT elements connected to both columns being pushed outwards. This increase in force in the PT elements will in turn induce compressive axial forces in the beam elements. Christopoulos [47] derived a relation that takes this behaviour at the beam-column connection into account and has been adapted for the SC-CBF described here. The PT force as a function of lateral roof displacement has been derived [62] as:

$$P_T = P_{T0} + 2k_{pt}\left(1 - \frac{1}{\Omega}\right)\frac{h_b\Delta}{H} \quad (11)$$

where  $\Omega$  is given by:

$$\Omega = 1 + \frac{k_b}{k_c + 2k_{pt}} \quad (12)$$

and  $k_b$ ,  $k_c$  and  $k_{pt}$  are the axial stiffness of the beam, flexural stiffness of the columns and axial stiffness of the PT elements, respectively. The final expression for the post-decompression stiffness of the PT frame is given in O'Reilly [62] for the SC-CBF shown in Fig. 3 as:

$$K_3 = 4k_{pt}\left(1 - \frac{1}{\Omega}\right)\frac{h_b^2}{H^2} \quad (13)$$

Examining the expression developed for  $K_3$  a little further, it is seen that  $K_3$  can be easily increased by increasing the axial stiffness of the PT elements, which can be achieved by increasing the cross-sectional area of the PT elements by increasing the number or diameter of strands. Since the secondary stiffness of a seismic resisting system influences the impact of P-Delta effects and degree to which residual drifts accumulate in structures without self-centring behaviour [65], the fact that this stiffness can be increased easily represents an additional advantage over conventional systems to aid the self-centring mechanism, where post-yield stiffnesses typically depend on material hardening ratios in conventional systems.

### 3. Experimental test setup

#### 3.1. Overview

The general layout of the SC-CBF test specimen is shown in Fig. 5. It consists of a single storey SC-CBF with PT elements located between the beam flanges above and below the storey containing braces, representative of an arbitrary storey in a multi-storey structure. Gravity loads from the floor slabs are assumed to pass through the central column and would not be directly carried by the beams that form part of the self-centring system. However, if the beams needed to carry gravity loads, then the additional forces in these beams and associated connections could be accounted for in their design. Care would need to be taken to ensure that connecting a floor slab to these beams would not restrict the frame forming the rocking connections. This section describes the test frame and the specific details associated with it, with reference to

**Table 1**

Details of diagonal brace specimens to be tested.

Specimen ID	Section Size	Grade	$\lambda_{zz}$	b/t
B0	None	–	–	–
B1A	20x20x2.0 SHS	S235	2.21	10
B1B				
B2A	25x25x2.5 SHS		1.70	10
B2B				
B3A	30x30x2.5 SHS		1.39	12
B3B				
B4A	40x40x4.0 SHS		1.03	10
B4B				

similar experimental programmes using a similar beam-column rocking connection detail.

### 3.2. Design of test frame

The complete design detail for the test frame shown in Fig. 5 can be found in O'Reilly [62], where a summary discussion is presented here. The test frame was sized so that it could be reused for multiple tests and, hence, the largest cross-section sizes were designed with reference to the maximum available actuator force available in the testing laboratory and also to ensure that the flag shape hysteretic behaviour was obtained for this section size. Using this combination of PT frame dimensions and initial axial force along with the largest brace specimens to ensure the self-centring behaviour illustrated in Fig. 4, the other brace sizes were also tested in this same frame.

#### 3.2.1. Brace specimens and gusset plates

Four grade S235 hot-rolled steel square hollow section sizes (SHS) manufactured in accordance with EN 10025:2004 [66] were selected for this experiment from catalogues of commercially available sections that would be compatible with the frame dimensions and capacity to ensure a self-centring behaviour. That is, with the moment frame dimensions and PT initial force selected based on material stress and strain limits (see Section 3.2.1), brace members were chosen so as to ensure the flag-shaped behaviour shown in Fig. 4 would result. Table 1 lists the braces tested and the corresponding  $\lambda_{zz}$  of each in the out-of-plane (OOP) direction (i.e. weak axis), using the nominal material properties. Each brace type had two specimens to be tested so as to maximise the data obtained during the test campaign, meaning eight specimen tests and one test without braces were conducted, giving a total of nine tests. For the calculation of the slenderness, an effective length coefficient of 1.0 was used, as suggested by Lehman *et al.* [23]. From Table 1, it can be seen that the  $\lambda_{zz}$  ranges from 1.03 to 2.21, covering the  $\lambda_{zz}$  range permitted by EC8, with the slenderest brace falling just outside the range. The width-to-thickness ( $b/t$ ) ratio of each brace was almost constant.

The gusset plate configuration was the same as that employed by Berman and Bruneau [67] where a brace is bolted, as opposed to welded,

to the beam only and is shown in Fig. 6. In this connection type, the gap opening of the beam-column connection is not restrained by the gusset plate welded in place to the surrounding frame and allows for specimens to be easily inserted and replaced. In order to ensure satisfactory behaviour and mitigate unwanted out-of-plane buckling of the gusset plates, a vertical stiffener was provided to replicate conventional gusset plates. These gusset plates were designed using the elliptical clearance method [24], whose details can be found in O'Reilly [62].

#### 3.2.2. Beam shear connection

Since the beams in the SC-CBF are allowed to rock freely against the face of the column and provide a self-centring mechanism, there should be no flexural resistance in the connection. However, the problem of transferring the shear force from the beams to the columns remains. In other similar systems, this shear force transfer relies on the frictional shear resistance between the beam flanges and the column face when compressed together. While there is some resistance provided at this friction interface, large shear forces from the vertical component of the brace axial forces to the columns need to be transferred. Therefore, a special shear tab (Fig. 6(b)) was designed to transfer this shear force from the beam to column. It was arranged in such a way to also permit the rotation of the beam against the column, via slotted bolt holes.

#### 3.2.3. Beam flange reinforcement

During rocking of the beam against the face of the column at maximum drift, there will be effectively one flange of the beam in contact with the column face. Hence, it was necessary to ensure that the beam flanges had adequate capacity to transfer the axial forces in the beams across the joint. This was done by adding reinforcing plates to the top and bottom of the beams, shown in Fig. 6. Previous experimental testing by Garlock [68] reported that local yielding in the beam flanges is detrimental to the intended behaviour of the self-centring frame. This is also true for the beam webs, where local yielding or buckling of the beam webs through their impact with the columns face will cause a sudden loss in PT force and thus the entire system. Winkley [69] mitigated this problem by keeping the beam webs away from the column face by inserting shim plates between the beam flanges and column face. An alternative method was employed in this test setup, where instead of inserting shim plates, an 8 mm notch was cut back into the beam web to keep it at a distance from the column face, as shown in Fig. 6.

#### 3.2.4. PT strands and anchorage

The spacing of the PT elements was also important; they were placed symmetrically about the centre of the beam to avoid any eccentric action. The spacing of the elements was important to not interfere with any of the other elements of the system, such as the beam shear tab. The PT strands selected consist of 7-wire standard strand with 12.5 mm nominal diameter typically used in concrete prestressing; details can be found in BS 5896:1980 [70]. These strands were chosen as they were a locally available typology that were identified as suitable in size for the test setup and were donated by a local contractor specialising in precast

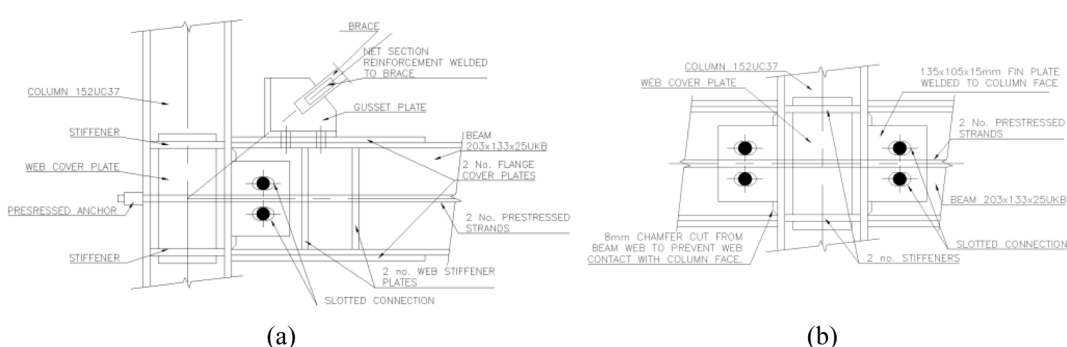


Fig. 6. Illustration of (a) the gusset plate connection details and (b) shear tab connection used in the SC-CBF test frame.



**Fig. 7.** SC-CBF test frame.

concrete services. The anchorage system used consisted of a set of grips that hold the PT strands in place and maintain the load, as typically in concrete prestressing strands. The initial force that installed in these strands was 80kN, as was deemed to be sufficient to demonstrate the flag shape for all specimens, but more refined values could have been chosen for specific brace arrangements. The specialised equipment needed to load the strands was not readily available in the laboratory and required the assistance of an external contractor. To avoid multiple requests and visits, a single initial force was utilised for all specimens for convenience. This initial force corresponded to 24% of the characteristic breaking load of the PT strands, given in BS 5896:1980. The force in the individual PT strands was measured using NovaTech F317 load cells [71], which reported the anchoring force between the strands and the frame. Their position is illustrated via the large purple attachments to

the strands on the left hand side of Fig. 5.

### 3.2.5. Base connection of the test frame

Since the test frame was a single storey SC-CBF substructure representative of an arbitrary storey in a multi-storey structure, one particular feature needed to be accommodated. Section 2.2 discussed the rocking connection used in a SC-CBF. It was highlighted that once the beam-column connection begins to open, the frame as a whole begins to expand laterally. Since the frame tested here was an arbitrary storey in a structure, this expansion needed to be accommodated. This is similar to the testing of a self-centring steel plate shear wall system by Winkley [69]. During this test programme of a single bay frame, one of the columns was restrained with a pinned connection and the other a pinned roller connection in the direction of loading. For the testing of the SC-CBF, a similar approach was adopted, where the two exterior columns were roller connections and the internal column was pinned.

### 3.3. Loading protocol

The loading protocol used for the testing of the specimens was a cyclic loading history defined by ECCS [72] typically used for steel brace specimens. Upon initial low-level displacement of the test frame, it was observed that there was a degree of looseness in either direction of the frame. The primary source of this looseness was in the connection of the base of the centre column to the adapter plate for the strong floor. Despite efforts to rectify this unintended looseness in the frame, an additional 5 mm was added to the displacement cycles in either direction to account for this.

## 4. Experimental results and observations

A total of nine tests were carried out on the test frame shown in Fig. 7. These consisted of eight brace specimens and one bare frame test,

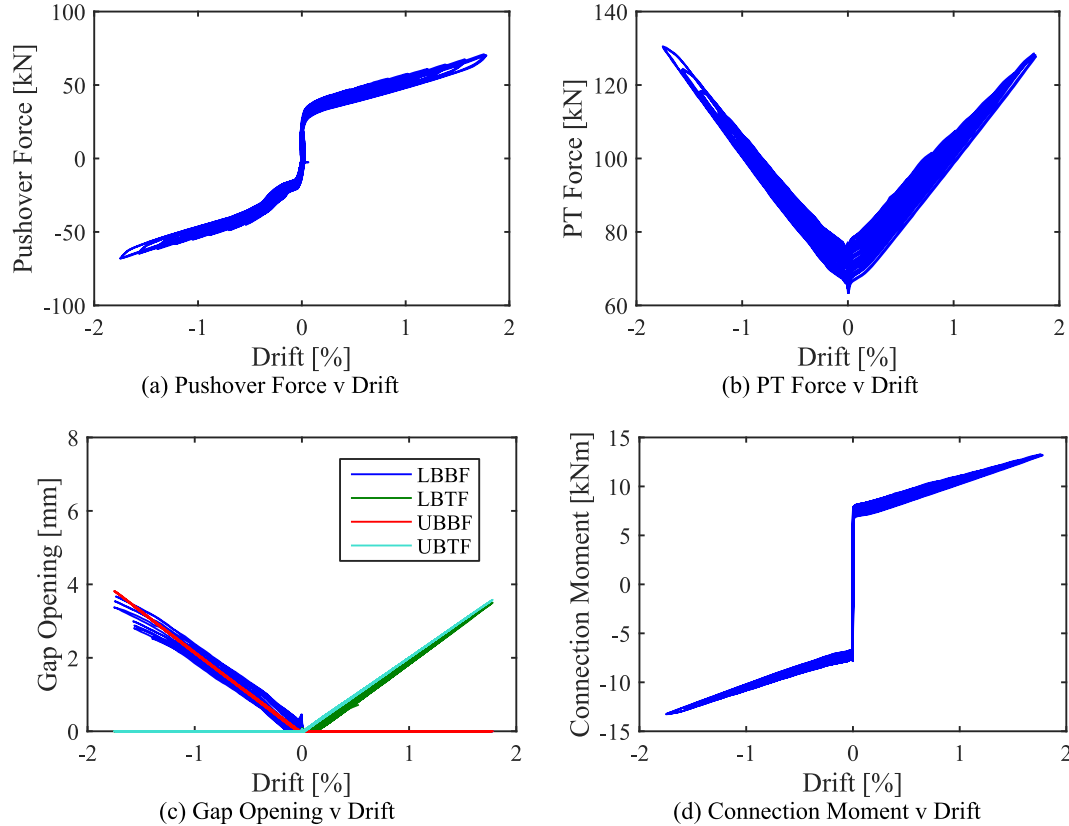


**Fig. 8.** B0 test results.

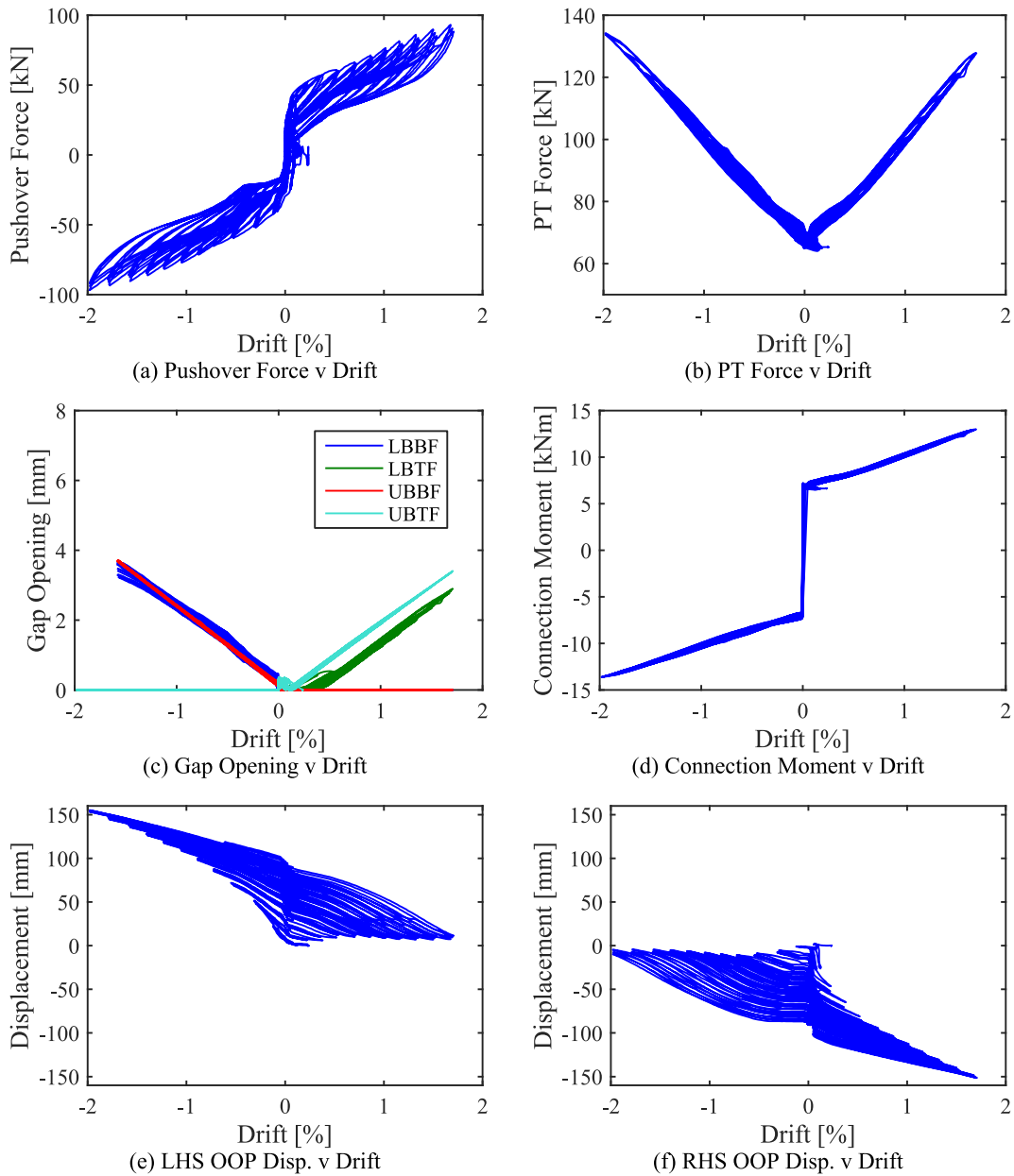


Fig. 9. B1A test results.

as listed in Table 1. This section will present the results from these tests and a summary will be given in Section 5. Hence, only a selection of plots is shown in the following sections, where detailed results for each specimen can be found in O'Reilly [62]. The abbreviations in the legends of the plots of the gap opening measurement refer to the position of the instruments on the frame: lower beam bottom flange (LBBF); lower beam top flange (LBTF); upper beam bottom flange (UBBF); and upper beam top flange (UBTF). This notation will be used throughout.

#### 4.1. Specimen B0

This test was performed to determine the behaviour of frame with the only PT elements installed and demonstrate the bilinear elastic behaviour of the frame. Fig. 8(a) shows a plot of the pushover force against drift of the frame, where the frame experienced a maximum drift of 1.78%. It can be seen that the hysteresis of the frame is a bilinear elastic response with very little energy dissipation. The small amount of area under the curves shown in Fig. 8(a) is due to the friction of the test

frame setup and slight relaxation of the PT strands initially shown in Fig. 8(b). This plot demonstrates the behaviour of the frame is as was anticipated, where the only difference is a slight unexpected kink in the response plot at approximately -0.25% drift. This behaviour occurred in only one direction of the testing and was not a characteristic of the self-centring frame, but rather a consequence of the test setup's manufacturing tolerances and the connection of the frame to the strong floor.

During this test, a degree of unintended movement in the test frame was observed. This was partly due to the pinned and roller connections at the base not being perfect pinned conditions. Efforts were made to reduce the effect, for example, by fabricating new pins with a tighter fit to reduce any initial looseness in the connection. However, a relatively small degree of flexibility persisted and was accounted for during the remaining tests. Secondly, it can be seen in Fig. 8(b) that the PT force in the strands is gradually decreasing during the test by roughly 5 to 10 kN. This was due to the frame being tested at high displacement cycles for the first time. The anchorage system employed for the PT strands were

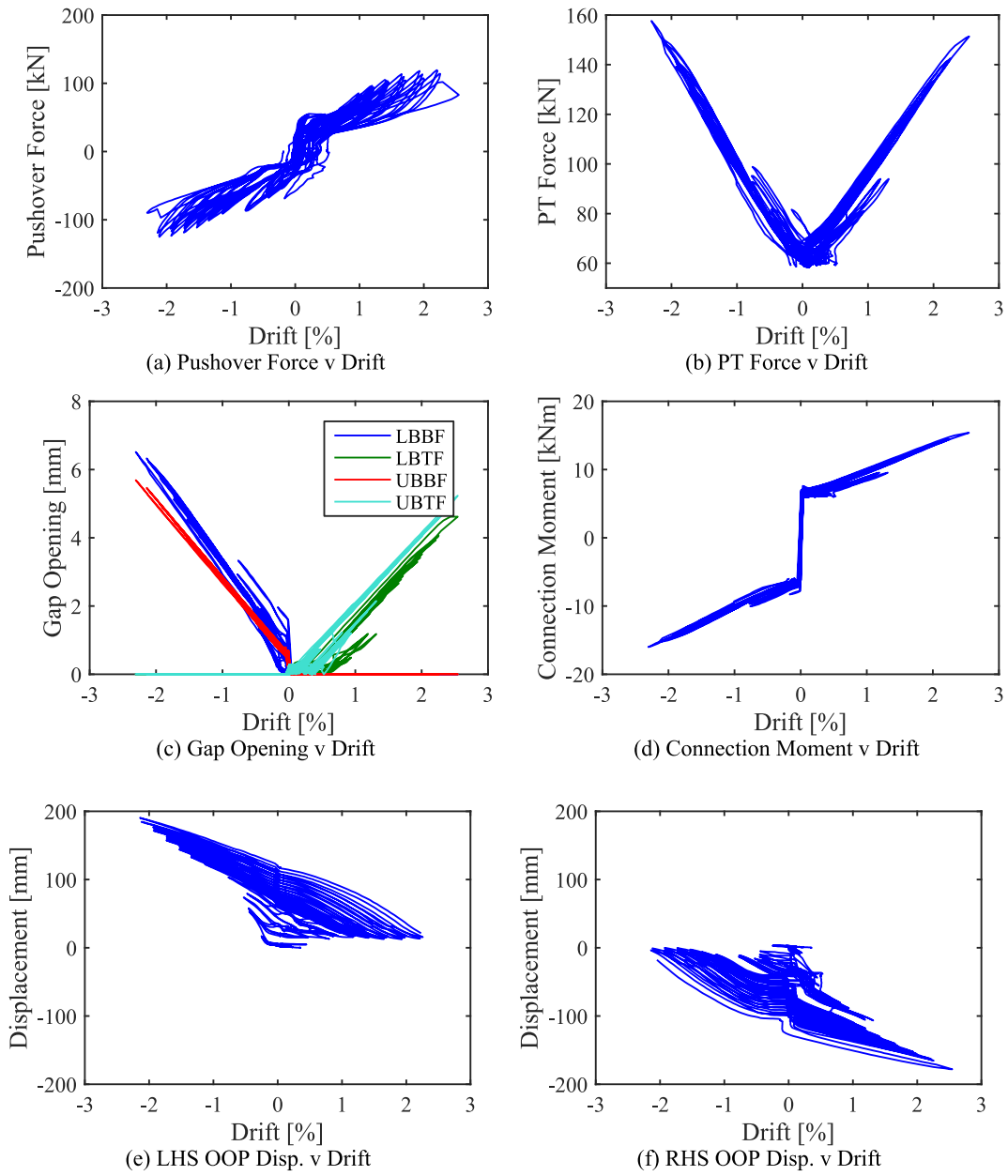


Fig. 10. B2B test results.

not rigidly attached to the frame and were fixed in place upon the application of the initial PT force. Initial testing and movement of the rocking connections likely shifted these anchors slightly to their final position, causing the initial reduction in PT force, which was not observed in the following test, as seen later.

#### 4.2. Specimen B1A

This was the first test carried out on the full SC-CBF frame consisting of both braces and self-centring frame system. During installation of the braces, the data acquisition system was set to record the installation and tightening of the bolts that connect the brace specimens to the test frame. This permitted quantification of any additional forces that may be induced in the specimens due to a lack of fit during the installation. For these specimens, the initial strains were of the order of  $195 \mu\epsilon$  and  $164 \mu\epsilon$  in the LHS and RHS braces, which equate to initial tensions force of 5.49 kN and 4.61 kN, respectively.

Fig. 9(a) shows the pushover force against drift, where it can be seen

that the flag-shaped behaviour of the self-centring frame is evident, in addition to the increase in lateral resistance and energy dissipation associated with the brace specimens. Again, it can be seen in Fig. 9(b) that the PT force increases as expected with drift. The gap opening of the connection causing the increase in PT force is shown in Fig. 9(c). The decompression moment required to achieve this gap opening is shown in Fig. 9(d) and the values remain unchanged from the previous B0 test, since the decompression moment is a function of the PT frame alone and is not influenced by the presence of the brace members. Fig. 9(e) and (f) show the OOP displacement of the left and right braces, respectively, which were measured using linear string potentiometers connected to the brace midpoints and positive denotes the direction out from the page in the diagram shown in Fig. 5. These plots are such that the two braces buckled in two different directions, but the peak OOP displacement at mid-length is the same for both braces. Initial buckling was observed in these braces at a storey drift of 0.13%, whereas the test labelled B1B not plotted here reported a buckling drift of 0.12%.

These test specimens did not fracture after the completed cycles and



**Fig. 11.** Gap opening of UBBF during B2B testing.

reported a drift of 1.71% in the positive direction and 1.98% in the negative direction. This unsymmetrical loading is observed in the test frame as the actuator position was not perfectly at the zero-stroke point before loading. Severe pinching can be seen in the hysteresis loops (Fig. 9(a)), as these braces represent the slenderest braces in the test setup. Pinching here refers to when the braces are reloading following a full cycle of deformation, the force does not follow and repeat the overall backbone response of the system to give a pure flag-shaped behaviour but rather gives a pinched loop with reduced hysteretic area, which is typical of more slender braces. These braces showed a residual OOP deformation after testing due to the many cycles of inelastic behaviour induced during testing, seen in Fig. 9(e) and (f). While this residual OOP deformation of the braces may provide some residual lateral resistance to the SC-CBF system, it is not expected to inhibit the self-centring mechanism of the SC-CBF system, so long as the conditions to ensure a flag-shaped hysteresis as shown in Fig. 4 are satisfied in the initial setup, as was the case for specimen B1A. In addition to this OOP displacement in the braces, some degree of necking (i.e. reduction in cross-sectional area) was observed after testing at the mid-point of both braces, although there was no evidence of any significant local buckling.

#### 4.3. Specimen B2B

Following the previous test, the specimens were removed and the next set could be installed for testing. For this B2B test, these were 25x25x2.5SHS brace sections. Fig. 10(a) shows the hysteresis of the frame where the specimen again exhibits a full flag shape loop with degrading loops due to the pinching of the braces. The same general trend with regard to the PT force, gap opening and connection moment is seen in Fig. 10(b) to (d), where the PT force increases with drift as expected, the gap opening of the beam column connection (Fig. 11) is similar to previously tests and symmetrical across the frame (i.e. connections with and without braces attached open and close as anticipated), and the connection moment due to the PT force also shows the bilinear elastic hysteresis. The brace OOP displacements shown in Fig. 10(e) and (f) show the expected trend, although the LHS brace displaces much further (by approximately 15%) than the RHS brace despite the frame being displaced to similar drifts in either direction (2.54% in the positive and 2.31% in the negative). The difference in OOP displacement could be due to the LHS brace not recovering as much straightness as the RHS brace during tensile loading, as can be seen in

Fig. 10(e), where a relatively large residual OOP displacement remains in the brace throughout the testing, especially when compared to the RHS brace. Initial buckling of these braces was observed at a storey drift of 0.45%. The necking of the RHS brace occurred at 1.95% drift in the positive direction, where tearing of both braces occurred during the second cycle of 2.54% in the positive direction and 2.31% in the negative direction. The LHS brace fully fractured first during the third cycle at this drift cycle, followed by the RHS brace in the reverse cycle.

#### 4.4. Specimen B3B

This was the second test performed on the 30x30x2.5SHS section size, where the salient response ordinates are given in Fig. 12. As before, this SC-CBF shows the expected flag-shaped behaviour in Fig. 12(a). From the plot of connection moment versus drift, it can be seen that the decompression moment has reduced slightly when compared to other tests. This is to be expected as a number of large amplitude cycles have been carried out on the specimens using the test frame; hence, a slight reduction in strand force is to be expected following many repeated cycles.

In addition to the trends that this test specimen showed similar to previous tests, other observations can be made from the plots in Fig. 12. These brace specimens are a stockier section size with a higher buckling capacity than the previous B1 and B2 specimens. From observation of the OOP displacement in Fig. 12(e) and (f), it can be seen that the OOP displacements are low during the initial cycles of small amplitude drift, but eventually increase quickly similar to the previous tests on the frames with more slender brace specimens. This was the same for both braces, where the corresponding drifts in Fig. 12(e) and (f) at which this observed buckling occurred are  $-0.95\%$  and  $+0.45\%$  for the LHS and RHS braces, respectively. Severe local buckling was observed in both braces during the first cycle of 2.20% drift and upon loading in tension in the reverse cycle, the RHS brace fractured fully. The LHS brace fractured later during the second cycle of 2.45% drift on the frame. Similar behaviour was observed during test B3A, as reported in Table 2.

#### 4.5. Specimen B4B

Fig. 13 shows a plot of the test results obtained from the B4B specimens. As expected, the test displayed the usual flag-shaped behaviour of the frame and self-centring. Similarly to the B3B specimen, the buckling of the braces after a few cycles of relatively little OOP displacement can be seen. The drift values at which this buckling occurred were  $-1.05\%$  and  $+1.10\%$  for the LHS and RHS braces, respectively. The recordings of positive drifts were again limited by the maximum displacement capacity of the LVDT documenting it.

As with the previous test on the B4 specimens, fracturing of the braces was not achieved. This was due to the actuator reaching its maximum stroke capacity and the frame could not be pushed any further to cause brace fracture. The final state of the test frame with the B4B specimens is shown in Fig. 14. Buckling of these braces occurred at storey drifts  $-1.18\%$  and  $+1.45\%$  for the LHS and RHS braces, respectively.

### 5. Discussion

#### 5.1. Summary of test results

Table 2 summarises salient response parameters for each test specimen, where the maximum and minimum drift values, pushover force and PT force in either direction are reported. The maximum absolute OOP displacements at the mid-length of both LHS and RHS braces are also listed for each brace specimen, with the exception of B2A where excessive noise in the recordings meant only a limited amount of data was available. Also presented in Table 2 is the total energy dissipated by each of the test specimens during testing, and also an indication of

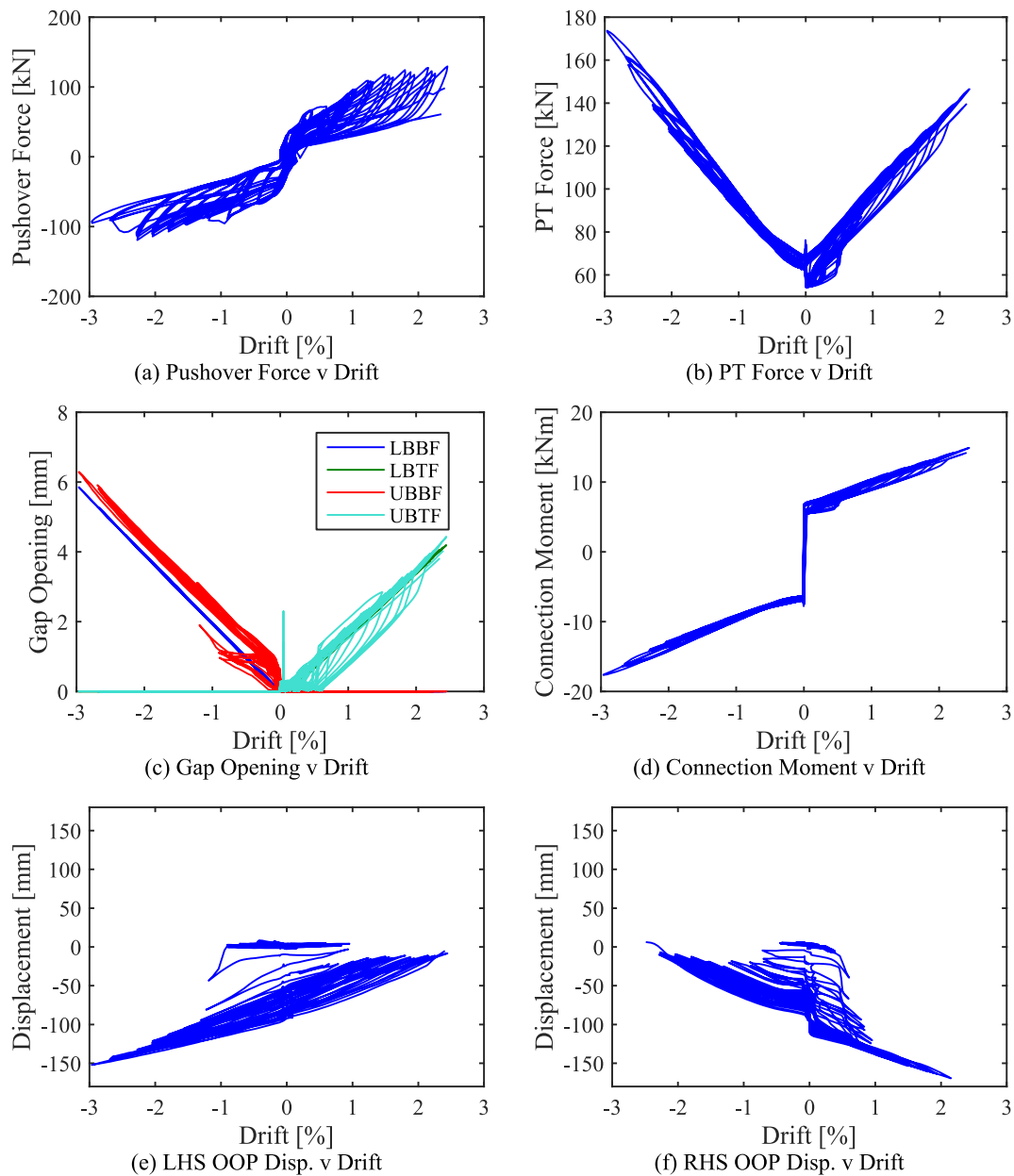


Fig. 12. B3B test results.

whether or not full fracture of the brace specimens occurred for each test. For the 3 specimens that did not report brace fracture, these are noted to be as a result of the actuator stroke limit not being able to push the specimens far enough into the non-linear range to cause brace fracture, as opposed to suggesting these specimens were fracture-resistant. The dissipated energy shows that the stockier braces, such as the B4B specimens, dissipates much more energy than the slenderer members due to the fatter hysteretic loops and the characteristic pinching behaviour of more slender members, reducing their total energy dissipation capacity. The energy dissipated up to a drift cycle of 1.5% was also computed and given in Table 2. Fig. 15 plots this versus the normalised slenderness of the brace members where braces with increased slenderness tended to dissipate less energy compared to stockier members. Also shown in Table 2 is the dissipated energy normalised by the elastic energy stored in the braces, where again, the difference in energy dissipation between the different normalised slenderness ratios is evident. Furthermore, in situations where instrument error or lack of suitable data was noted, the corresponding data was

either estimated visually from available results (as in the case of OOP displacements of specimens B3A and B4A where noise was present in the data) or not included in Table 2 to avoid any erroneous conclusions, as noted in the table footnotes.

### 5.2. Comparison with analytical predictions

The maximum PT force for each of the test specimens is shown in Table 2 for both the positive and negative drift cycles imposed on the frame. The maximum PT force measured in the test specimens was 64.7% of the nominal tension yield resistance of the PT strands. Thus, the objective of limiting the strand forces to less than 75% the nominal strength was achieved. These values observed in the tests can be compared to those predicted by the expression developed for PT force in Eq. (11). This comparison is shown in Fig. 16(a) via a percentage difference from the observed value. It shows a difference less than 10% for all but two tests, where B4A and B4B fell outside this range but still within 20%.

**Table 2**

Summary of test results.

Specimen ID		B0	B1A	B1B	B2A <sup>b</sup>	B2B	B3A <sup>c</sup>	B3B	B4A <sup>c</sup>	B4B
Drift (+)	[%]	1.78	1.71	2.23	1.35	2.54	2.63	2.52	3.37	2.66
Drift (-)	[%]	-1.75	-1.98	-2.05	-1.69	-2.31	-2.07	-2.97	-3.4	-2.76
Pushover Force (+)	[kN]	70.9	93.2	107.4	112.5	119.4	129.4	129.5	204.6	192.2
Pushover Force (-)	[kN]	-68.1	-96.8	-108.5	-113.3	-125	-121.6	-119.3	-215.6	-180.7
PT Force (+)	[kN]	129.8	127.8	146.1	115.8	151.4	160.5	163.1	169.5	148.9
PT Force (-)	[kN]	130.5	133.9	151.1	120.5	157.6	160.3	173.7	166.4	143.6
LHS OOP	[mm]	-	155.1	162.2	-	190.3	156.9	152.1	197.4	139.0
RHS OOP	[mm]	-	151.4	166.5	-	165.6	163.4	169.3	160.5	140.7
Fracturing <sup>d</sup>	-/-	-/-	L/R	-/R	L/R	L/R	L/R	-/-	-/-	-/-
Total Dissipated Energy	[kNm]	2.31	7.72	10.43	-	14.61	16.64	18.05	71.93	50.98
Dissipated Energy <sup>a</sup>	[kNm]	-	2.1	4.9	-	7.6	10.35	11.43	14.64	17.18
Dissipated/Elastic	-	-	26.86	62.59	-	49.91	59.39	65.57	37.84	44.38
$M_c$ (+)	[kNm]	7.2	6.5	6.2	6.5	6.2	6.1	5.6	5.7	5.3
$M_c$ (-)	[kNm]	-7.3	-6.9	-6.5	-6.6	-6.6	-6.3	-5.7	-5.7	-5.6
$M_{c,max}$ (+)	[kNm]	13.2	13	14.1	11.7	16.4	15.9	14.8	14.8	13.8
$M_{c,max}$ (-)	[kNm]	-13.3	-13.6	-14.8	-12.3	-16	-14.4	-16.8	-16.9	-14.6
$k_r^0$ (+)	[kNm]	339	382.4	399	383.8	400.8	379.8	375.5	321.6	328.2
$k_r^0$ (-)	[kNm]	340.6	339.9	392.9	330.4	407.4	391.3	373.3	339.4	326.1

a. Energy dissipated up to 3 cycles nearest 1.5% drift.

b. Values represent a limited amount of data due to limited data available from test.

c. Brace OOP data estimated visually due to noise present in OOP data logging.

d. L/R indicates full fracture in both LHS and RHS brace whereas -/- indicates no fracturing of either.

The post-decompression stiffness with respect to the connection rotation of the self-centring frame,  $k_r^0$ , was calculated in both directions for each test using the decompression moment,  $M_c$ , and the maximum connection moment,  $M_{c,max}$ , given in Table 2. These are compared to the prediction equation derived from  $K_3$  in Eq. (13) as:

$$k_r^0 = k_{pi} \left( 1 - \frac{1}{\Omega} \right) h_b^2 \quad (14)$$

The percentage difference between the test values and the prediction are shown in Fig. 16(b), where the observed values fall within 15% of the calculated value, confirming the suitability of Eq. (13) for in determining the  $K_3$  of the frame.

The maximum absolute OOP displacements of the braces are also shown in Table 2. These can be compared to a simple expression to predict the OOP brace displacement by Tremblay [13], given by:

$$\Delta_{OOP} = \frac{1}{\sqrt{2}} \sqrt{\Delta_a L} \quad (15)$$

where  $\Delta_{OOP}$  is the OOP displacement,  $L$  is the length of the brace and  $\Delta_a$  is the axial displacement of the brace, which, by following the same process outlined in Eq. (2) to Eq. (6), can be shown to be equal to  $\theta BH/L$ , where  $\theta$  denotes the drift. Fig. 16(c) shows the percentage difference for each of the tests except B0 and B2A for the reasons noted in Table 2. Fig. 16 shows that, in general, Eq. (15) tends to underestimate the maximum OOP displacement of the braces but the predicted values are still within approximately 20% of the observed test values.

## 6. Summary and conclusions

A novel self-centring concentrically braced frame (SC-CBF) system was developed and tested through laboratory cyclic push-over tests. This was done by combining the existing CBF arrangement with a rocking connection to give a system that dissipates energy as a conventional CBF, but also demonstrates a self-centring behaviour following many cycles of inelastic deformation. This concept was developed to describe the hysteretic behaviour of the novel system to lateral loading. An experimental programme was presented to test and validate this concept using a variety of tubular brace sections subject to quasi-static cyclic loading.

The results of the experimental testing showed that the SC-CBF demonstrates the bilinear elastic behaviour, typical of self-centring systems that utilise the rocking connection, when first tested without

any brace specimens. This validated the rocking connection behaviour which was then combined with diagonal steel brace members, where the lateral capacity was greatly increased. The specimens were tested under many cycles of inelastic deformation up to brace fracture with a maximum storey drift at brace fracture of 3.4% noted. The tests demonstrated how the anticipated gap opening behaviour occurred at each of the beam column connections, causing an increase in the PT force with increasing drift. This increase in PT force was also noted for both directions of loading, as well as the bilinear elastic moment rotation behaviour of each beam-column connection to further demonstrate the re-centring behaviour of the frame.

The test results were compared to the analytical expressions developed to describe the behaviour of the SC-CBF. A comparison of the maximum PT force showed that the analytical predictions were within 10% of the actual value, except for two tests where the difference was still within 20%.

The post decompression stiffness of the frame was then derived and compared to the expression developed previously. The comparison showed that the predictions were within 15% of the actual observed test values. This demonstrated the validity of the expressions derived to describe the self-centring behaviour of the PT frame.

The out-of-plane displacements of the braces were compared to a simple expression available in the literature for conventional CBFs. The results showed that the OOP predictions for the braces were within 20% of the actual value, demonstrating that the brace members do indeed perform in the same fashion to conventional CBF members.

The energy dissipated by each of the brace specimens was calculated up to a drift cycle of 1.5% and plotted versus normalised slenderness, showing that the energy dissipation of the braces decreased with increasing normalised slenderness. This is to be expected due to the large pinching in the hysteretic behaviour of more slender members typically observed in CBFs.

Considering these observations regarding the overall response of the SC-CBF test frame to lateral loading and the comparisons made with analytical prediction, this study validates the structural performance of the SC-CBF. Future work also envisages the calibration of numerical models to accurately quantify the response, along with shake table testing and the development of a procedure to design and implement such the structural system in practice.

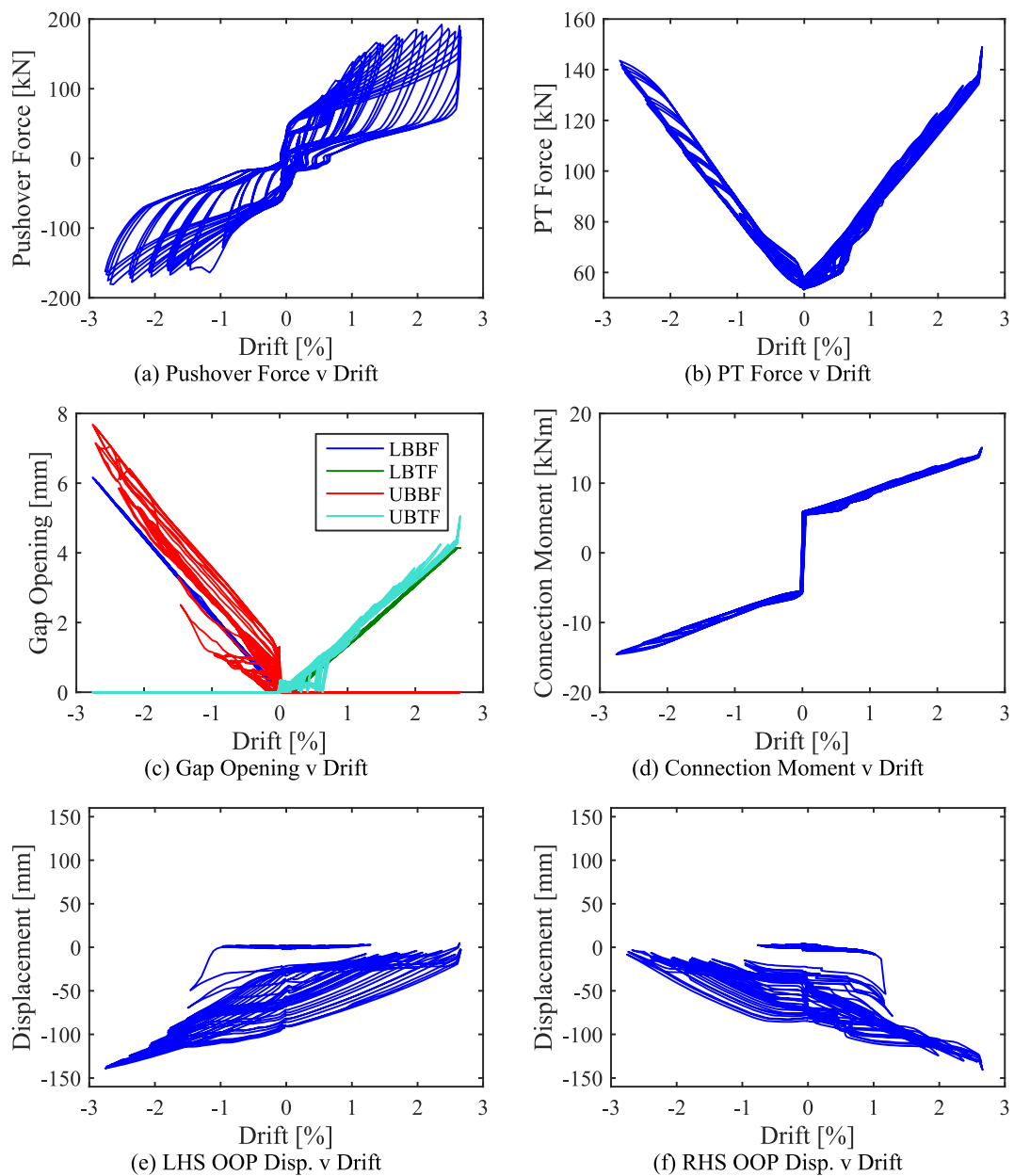


Fig. 13. B4B test results.



Fig. 14. B4B specimens after testing.

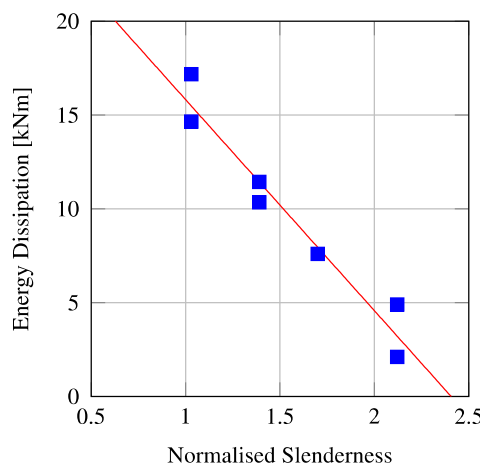


Fig. 15. Energy dissipation to 1.5% versus normalised slenderness.

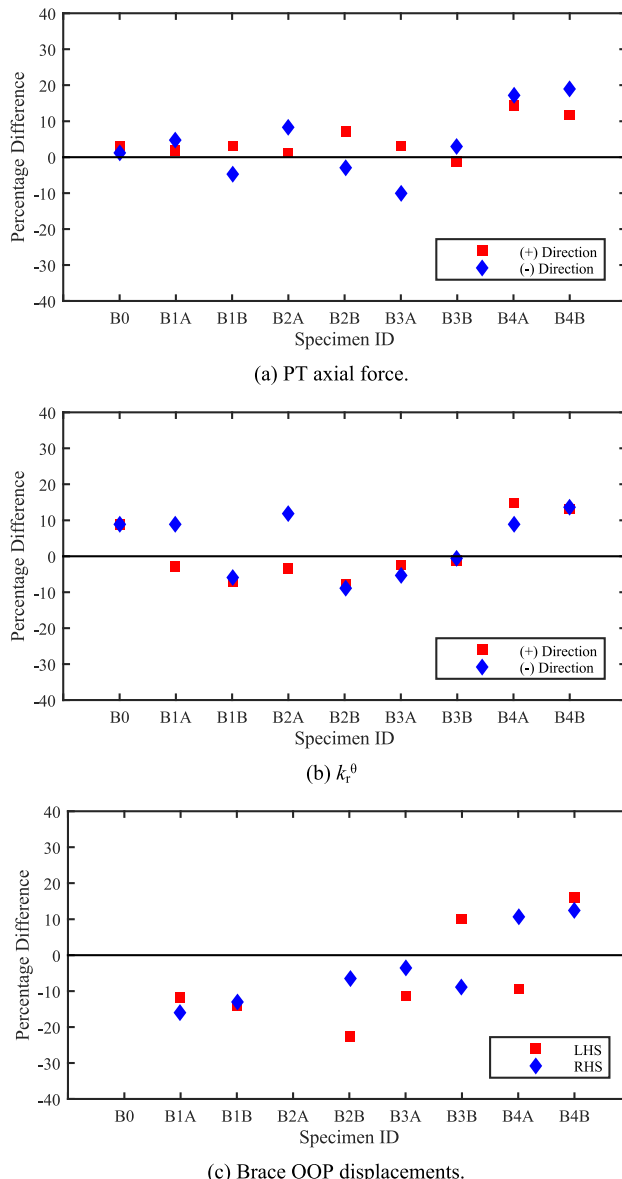


Fig. 16. Percentage difference of observed and predicted response parameters for each test.

## CRediT authorship contribution statement

**Gerard J. O'Reilly:** Conceptualization, Methodology, Resources, Software, Validation, Writing - original draft. **Jamie Goggins:** Conceptualization, Validation, Writing - review & editing, Supervision.

## Declaration of Competing Interest

The authors declare that they have no known competing financial interests or personal relationships that could have appeared to influence the work reported in this paper.

## Acknowledgements

The first author gratefully acknowledges the funding provided by the Irish Research Council. The material and services provided by Oran Precast Ltd. in the setup of the post-tensioning arrangement of the test frame is also gratefully acknowledged.

## References

- [1] CEN. Eurocode 8: Design of Structures for Earthquake Resistance - Part 1: General Rules, Seismic Actions and Rules for Buildings (EN 1998-1:2004). Brussels, Belgium: 2004.
- [2] O'Reilly GJ, Calvi GM. Conceptual seismic design in performance-based earthquake engineering. *EARTHQ ENG Struct Dyn* 2019;48:389–411. <https://doi.org/10.1002/eqe.3141>.
- [3] O'Reilly GJ, Calvi GM. Quantifying seismic risk in structures via simplified demand-intensity models. *Bull Earthq Eng* 2020;18:2003–22. <https://doi.org/10.1007/s10518-019-00776-0>.
- [4] Khatib IF, Mahin SA, Pister KS. *Seismic Behavior of Concentrically Braced Steel Frames*. Report No. UCB/EERC-88/01. Berkeley: California; 1988.
- [5] Salawdeh S, Goggins J. Performance based design approach for multi-storey concentrically braced steel frames. *Steel Compos Struct* 2016;20:749–76. <https://doi.org/10.12989/scs.2016.20.4.749>.
- [6] Salawdeh S, Goggins J. Direct displacement based seismic design for single storey steel concentrically braced frames. *Earthquakes Struct* 2016;10:1125–41. <https://doi.org/10.12989/eas.2016.10.5.1125>.
- [7] Hunt A. *Design and Analysis of Concentrically Braced Steel Frames under Seismic Loading*. Trinity College Dublin; 2013. PhD Thesis.
- [8] Salawdeh S, Ryan T, Broderick BM, Goggins J. DDBD assessment of steel CBFs using full scale shake table tests with realistic connections. *J Constr Steel Res* 2019; 154:14–26. <https://doi.org/10.1016/j.jcsr.2018.11.022>.
- [9] O'Reilly GJ, Sullivan TJ. Fragility Function for Eccentrically Braced Frame Structures. *Earthquakes Struct* 2016;10:367–88. <https://doi.org/10.12989/eas.2016.10.2.367>.
- [10] O'Reilly GJ, Sullivan TJ. Direct Displacement-Based Seismic Design of Eccentrically Braced Steel Frames. *J Earthq Eng* 2016;20:243–78. <https://doi.org/10.1080/13632469.2015.1061465>.
- [11] Sabelli R, Roeder CW, Hajjar JF. *Seismic design of steel special concentrically braced frame systems: a guide for practicing engineers*. NEHRP Seism Des Tech Br No 2013;8.
- [12] Goggins J, Broderick BM, Elghazouli AY, Lucas AS. Experimental cyclic response of cold-formed hollow steel bracing members. *Eng Struct* 2005;27:977–89. <https://doi.org/10.1016/j.engstruct.2004.11.017>.
- [13] Tremblay R. Inelastic seismic response of steel bracing members. *J Constr Steel Res* 2002;58:665–701. [https://doi.org/10.1016/S0143-974X\(01\)00104-3](https://doi.org/10.1016/S0143-974X(01)00104-3).
- [14] Nip KH, Gardner L, Davies CM, Elghazouli AY. Extremely low cycle fatigue tests on structural carbon steel and stainless steel. *J Constr Steel Res* 2010;66:96–110. <https://doi.org/10.1016/j.jcsr.2009.08.004>.
- [15] Nip KH, Gardner L, Elghazouli AY. Cyclic testing and numerical modelling of carbon steel and stainless steel tubular bracing members. *Eng Struct* 2010;32: 424–41. <https://doi.org/10.1016/j.engstruct.2009.10.005>.
- [16] Haddad M, Brown T, Shrive N. Experimental cyclic loading of concentric HSS braces. *Can J Civ Eng* 2011;38:110–23. <https://doi.org/10.1139/L10-113>.
- [17] Gardner L, Saari N, Wang F. Comparative experimental study of hot-rolled and cold-formed rectangular hollow sections. *Thin-Walled Struct* 2010;48:495–507. <https://doi.org/10.1016/j.tws.2010.02.003>.
- [18] Han S-W, Kim WT, Foutch DA. Seismic Behavior of HSS Bracing Members according to Width-Thickness Ratio under Symmetric Cyclic Loading. *J Struct Eng* 2007;133:264–73. [https://doi.org/10.1061/\(ASCE\)0733-9445\(2007\)133:2\(264\)](https://doi.org/10.1061/(ASCE)0733-9445(2007)133:2(264)).
- [19] Elchalakani M, Zhao X-L, Grzebietka R. Tests of Cold-Formed Circular Tubular Braces under Cyclic Axial Loading. *J Struct Eng* 2003;129:507–14. [https://doi.org/10.1061/\(ASCE\)0733-9445\(2003\)129:4\(507\)](https://doi.org/10.1061/(ASCE)0733-9445(2003)129:4(507)).
- [20] Santagati S, Bolognini D, Nascimbene R. Strain Life Analysis at Low-Cycle Fatigue on Concentrically Braced Steel Structures with RHS Shape Braces. *J Earthq Eng* 2012;16:107–37.
- [21] Salawdeh S, Goggins J. Numerical simulation for steel brace members incorporating a fatigue model. *Eng Struct* 2013;46:332–49. <https://doi.org/10.1016/j.engstruct.2012.07.036>.

- [22] Hassan MS, Salawdeh S, Goggins J. Determination of geometrical imperfection models in finite element analysis of structural steel hollow sections under cyclic axial loading. *J Constr Steel Res* 2018;141:189–203. <https://doi.org/10.1016/j.jcsr.2017.11.012>.
- [23] Lehman DE, Roeder CW, Herman D, Johnson S, Kotulka B. Improved Seismic Performance of Gusset Plate Connections. *J Struct Eng* 2008;134:890–901. [https://doi.org/10.1061/\(ASCE\)0733-9445\(2008\)134:6\(890\)](https://doi.org/10.1061/(ASCE)0733-9445(2008)134:6(890)).
- [24] Roeder CW, Lumpkin EJ, Lehman DE. A balanced design procedure for special concentrically braced frame connections. *J Constr Steel Res* 2011;67:1760–72. <https://doi.org/10.1016/j.jcsr.2011.04.016>.
- [25] Salawdeh S, English J, Goggins J, Elghazouli AY, Hunt A, Broderick BM. Shake table assessment of gusset plate connection behaviour in concentrically braced frames. *J Constr Steel Res* 2017;138:432–48. <https://doi.org/10.1016/j.jcsr.2017.07.022>.
- [26] Goggins J, Broderick BM, Elghazouli AY, Salawdeh S, Hunt A, Mongabure P, et al. Shake Table Testing of Concentrically Braced Steel Structures With Realistic Connection Details Subjected to Earthquakes. *Structures* 2018;13:102–18. <https://doi.org/10.1016/j.istruc.2017.12.003>.
- [27] Yoo JH, Lehman DE, Roeder CW. Influence of connection design parameters on the seismic performance of braced frames. *J Constr Steel Res* 2008;64:607–23. <https://doi.org/10.1016/j.jcsr.2007.11.005>.
- [28] Roeder CW, Lehman DE, Clark K, Powell J, Yoo J-H, Tsai K-C, et al. Influence of gusset plate connections and braces on the seismic performance of X-braced frames. *Earthq Eng Struct Dyn* 2011;40:355–74. <https://doi.org/10.1002/eqe.1024>.
- [29] Shaback B, Brown T. Behaviour of square hollow structural steel braces with end connections under reversed cyclic axial loading. *Can J Civ Eng* 2003;30:745–53. <https://doi.org/10.1139/I03-028>.
- [30] Lin P-C, Tsai K-C, Wu A-C, Chuang M-C. Seismic design and test of gusset connections for buckling-restrained braced frames. *Earthq Eng Struct Dyn* 2014;43: 565–87. <https://doi.org/10.1002/eqe.2360>.
- [31] Lin P-C, Tsai K-C, Wu A-C, Chuang M-C, Li C-H, Wang K-J. Seismic design and experiment of single and coupled corner gusset connections in a full-scale two-story buckling-restrained braced frame. *Earthq Eng Struct Dyn* 2015;44:2177–98. <https://doi.org/10.1002/eqe.2577>.
- [32] Broderick BM, Elghazouli AY, Goggins J. Earthquake testing and response analysis of concentrically-braced sub-frames. *J Constr Steel Res* 2008;64:997–1007. <https://doi.org/10.1016/j.jcsr.2007.12.014>.
- [33] Broderick BM, Goggins J, Beg D, Elghazouli AY, Mongabure P, Le Maoult A, et al. Assessment of the Seismic Response of Concentrically-Braced Steel Frames. In: Taucer F, Apostolska R, editors. *Exp. Res. Earthq. Eng. Geotech. Geol. Earthq. Eng.* 35th ed., Patras, Greece: 2015, p. 327–44. Doi: 10.1007/978-3-319-10136-1\_20.
- [34] Okazaki T, Lignos DG, Hikino T, Kajiwara K. Dynamic Response of a Chevron Concentrically Braced Frame. *J Struct Eng* 2013;139:515–25. [https://doi.org/10.1061/\(ASCE\)ST.1943-541X.0000679](https://doi.org/10.1061/(ASCE)ST.1943-541X.0000679).
- [35] Shaw SM, Kanvinde AM, Fell BV. Earthquake-induced net section fracture in brace connections – experiments and simulations. *J Constr Steel Res* 2010;66:1492–501. <https://doi.org/10.1016/j.jcsr.2010.06.002>.
- [36] Yoo JH, Roeder CW, Lehman DE. Analytical Performance Simulation of Special Concentrically Braced Frames. *J Struct Eng* 2008;134:881–9. [https://doi.org/10.1061/\(ASCE\)0733-9445\(2008\)134:6\(881\).1](https://doi.org/10.1061/(ASCE)0733-9445(2008)134:6(881).1).
- [37] Hammad A, Moustafa MA. Shake table tests of special concentric braced frames under short and long duration earthquakes. *Eng Struct* 2019;200. <https://doi.org/10.1016/j.engstruct.2019.10965>.
- [38] Chen Y, Wang W, Chen Y. Full-scale shake table tests of the tension-only concentrically braced steel beam-through frame. *J Constr Steel Res* 2018;148: 611–26. <https://doi.org/10.1016/j.jcsr.2018.06.017>.
- [39] McCormick J, Aburano H, Ikenaga M, Nakashima M. Permissible residual deformation levels for building structures considering both safety and human elements. 14th World Conf. Earthq. Eng., Beijing, China: 2008.
- [40] FEMA P-58-1. *Seismic Performance Assessment of Buildings. Methodology* 2012; 11.
- [41] O'Reilly GJ, Perrone D, Fox M, Monteiro R, Filiatrault A. Seismic assessment and loss estimation of existing school buildings in Italy. *Eng Struct* 2018;168:142–62. <https://doi.org/10.1016/j.engstruct.2018.04.056>.
- [42] Elwood KJ, Marquis F, Kim JH. Post-Earthquake Assessment and Repairability of RC Buildings: Lessons from Canterbury and Emerging Challenges. Proc Tenth Pacific Conf Earthq Eng, Sydney, Australia: 2015.
- [43] EN 1090-2:2018. Execution of steel structures and aluminium structures. Technical requirements for steel structures 2018.
- [44] Stanton J, Stone WC, Cheok GS. *A Hybrid Reinforced Precast Frame for Seismic Regions. PCI J* 1997;March-April:20–32.
- [45] Ricles JM, Sause R, Garlock MM, Zhao C. Posttensioned Seismic-Resistant Connections for Steel Frames. *J Struct Eng* 2001;127:113–21. [https://doi.org/10.1061/\(ASCE\)0733-9445\(2001\)127:2\(113\).1](https://doi.org/10.1061/(ASCE)0733-9445(2001)127:2(113).1).
- [46] Garlock MM, Ricles JM, Sause R. Experimental Studies of Full-Scale Posttensioned Steel Connections. *J Struct Eng* 2005;131:438–48. [https://doi.org/10.1061/\(ASCE\)0733-9445\(2005\)131:3\(438\).1](https://doi.org/10.1061/(ASCE)0733-9445(2005)131:3(438).1).
- [47] Christopoulos C. *Self-Centering Post-Tensioned Energy Dissipating Steel Frames For Seismic Regions*. San Diego: University of California; 2002. PhD Thesis.
- [48] Christopoulos C, Tremblay R, Kim HJ, Lacerte M. Self-Centering Energy Dissipative Bracing System for the Seismic Resistance of Structures: Development and Validation. *J Struct Eng* 2008;134:96–107. [https://doi.org/10.1061/\(ASCE\)0733-9445\(2008\)134:1\(96\).1](https://doi.org/10.1061/(ASCE)0733-9445(2008)134:1(96).1).
- [49] Clayton PM, Berman JW, Lowes LN. Seismic Design and Performance of Self-Centering Steel Plate Shear Walls. *J Struct Eng* 2012;138:22–30. [https://doi.org/10.1061/\(ASCE\)ST.1943-541X.0000421](https://doi.org/10.1061/(ASCE)ST.1943-541X.0000421).
- [50] Nobahar E, Asgarian B, Mercan O, Soroushian S. A post-tensioned self-centering yielding brace system: development and performance-based seismic analysis. *Struct Infrastruct Eng* 2020;1–21. <https://doi.org/10.1080/15732479.2020.1572262>.
- [51] Kammula V, Erochko J, Kwon O, Christopoulos C. V. Kammula, J. Erochko, O. Kwon, C. Christopoulos, Performance Assessment of the Self Centering Energy Dissipative (SCED) Bracing System using Hybrid Simulation. 15th World Conf. Earthq. Eng., Lisbon, Portugal: 2012.
- [52] Erochko J, Christopoulos C, Tremblay R, Kim H-J. Shake table testing and numerical simulation of a self-centering energy dissipative braced frame. *Earthq Eng Struct Dyn* 2013;42:1617–35. <https://doi.org/10.1002/eqe.2290>.
- [53] Erochko J, Christopoulos C, Tremblay R. Design, Testing, and Detailed Component Modeling of a High-Capacity Self-Centering Energy-Dissipative Brace. *J Struct Eng* 2015;141:04014193. [https://doi.org/10.1061/\(ASCE\)ST.1943-541X.0001166](https://doi.org/10.1061/(ASCE)ST.1943-541X.0001166).
- [54] Xu L, Fan X, Li Z. Hysteretic Analysis Model for Pre-pressed Spring Self-Centering Energy Dissipation Braces. *J Struct Eng* 2018;144:04018073. [https://doi.org/10.1061/\(ASCE\)ST.1943-541X.0002060](https://doi.org/10.1061/(ASCE)ST.1943-541X.0002060).
- [55] Xu L, Fan X, Li Z. Seismic Assessment of Buildings with Prepressed Spring Self-Centering Energy Dissipation Braces. *J Struct Eng* 2020;146:04019190. [https://doi.org/10.1061/\(ASCE\)ST.1943-541X.0002493](https://doi.org/10.1061/(ASCE)ST.1943-541X.0002493).
- [56] Fan X-W, Xu L-H, Xie X-S, Sun Y-S, Li Z-X. Hysteresis analysis of pre-pressed spring self-centering energy dissipation braces using different models. *Adv Struct Eng* 2019;22:2662–71. <https://doi.org/10.1177/1369433219849844>.
- [57] Chi P, Tian W, Guo T, Cao D, Dong J. Parametric Study on the Seismic Response of Steel-Framed Buildings with Self-Centering Tension-Only Braces. *Adv Civ Eng* 2019;2019:1–17. <https://doi.org/10.1155/2019/9204362>.
- [58] Zhu S, Zhang Y. Seismic behaviour of self-centring braced frame buildings with reusable hysteretic damping brace. *Earthq Eng Struct Dyn* 2007;36:1329–46. <https://doi.org/10.1002/eqe.683>.
- [59] Roke DA, Sause R, Ricles JM, Gonner N. Design Concepts for Damage-Free Seismic Resistant Self-Centering Concentrically-Braced Frames. 14th World Conf. Earthq. Eng., vol. 1, Beijing, China: 2008.
- [60] Roke D, Sause R, Ricles JM, Chancellor B. Damage-free seismic-resistant self-centering concentrically-braced frames. *ATLSS Rep No* 2010;10–109.
- [61] Christopoulos C, Filiatrault A, Uang CM, Folz B. Posttensioned Energy Dissipating Connections for Moment-Resisting Steel Frames. *J Struct Eng* 2002;128:1111–20. [https://doi.org/10.1061/\(ASCE\)0733-9445\(2002\)128:9\(111\).1](https://doi.org/10.1061/(ASCE)0733-9445(2002)128:9(111).1).
- [62] O'Reilly GJ. Development of a Novel Self-Centering Concentrically Braced Steel Frame System. Galway: National University of Ireland; 2013. MSc Thesis.
- [63] O'Reilly G, Goggins J. Comparing the seismic performance of concentrically braced frames with and without self-centering behaviour. *Struct. Archit.*, Guimaraes, Portugal: CRC Press; 2013, p. 1540–7. Doi: 10.1201/b15267-213.
- [64] Goggins J, Broderick BM, Elghazouli AY, Lucas AS. Behaviour of tubular steel members under cyclic axial loading. *J Constr Steel Res* 2006;62:121–31. <https://doi.org/10.1016/j.jcsr.2005.04.012>.
- [65] Kawashima K, MacRae GA, Hoshikuma J, Nagaya K. Residual Displacement Response Spectrum. *J Struct Eng* 1998;124:523–30. [https://doi.org/10.1061/\(ASCE\)0733-9445\(1998\)124:5\(523\).1](https://doi.org/10.1061/(ASCE)0733-9445(1998)124:5(523).1).
- [66] EN 10025-2:2004. European structural steel standard: Grade designations, properties and nearest equivalents 2004.
- [67] Berman JW, Bruneau M. Cyclic Testing of a Buckling Restrained Braced Frame with Unconstrained Gusset Connections. *J Struct Eng* 2009;135:1499–510. [https://doi.org/10.1061/\(ASCE\)ST.1943-541X.0000078](https://doi.org/10.1061/(ASCE)ST.1943-541X.0000078).
- [68] Garlock MM. Design, Analysis, and Experimental Behavior of Seismic Resistant Post-Tensioned Steel Moment Resisting Frames. Lehigh University; 2002. PhD Thesis.
- [69] Winkley TB. *Self-Centering Steel Plate Shear Walls: Large Scale Experimental Investigation*. University of Washington; 2011.
- [70] BSI. BS 5896:1980: Specification for: High tensile steel wire and strand for the prestressing of concrete. London, UK: 1980.
- [71] Novatech. F317 High Performance Fatigue Rated Cylindrical Loadcell 2020. <https://www.novatechloadcells.co.uk/product-pdf/f317> (accessed August 25, 2020).
- [72] ECCS. Recommended Testing Procedure for Assessing the Behaviour of Structural Steel Elements under Cyclic Loads. 1986.